Influence of groundwater on present and past climate

By Ducharne A, Colin J, Decharme B, Cheruy F, Ghattas J, P Arboleda, Lo MH.

March 6th, 2020

1. Introduction

Groundwater (GW) constitutes by far the largest volume of liquid freshwater on Earth. The most active part is soil moisture (SM), recognized as a key variable of land/atmosphere interactions, especially in so-called transition zones, where/when SM varies between wet and dry values (Koster et al., 2004; Seneviratne et al., 2010; Cheruy et al., 2014). But GW can also be stored in deeper reservoirs than soils, in particular unconfined aquifer systems, in which the saturated part is called the water table. The latter is characterized by slow and mostly horizontal water flows towards the river network, with well-known buffering effects on streamflow variability (e.g. Gascoin et al., 2009). Where/when the water table is shallow enough, it can also sustain SM by means of capillary rise, thus increase evapotranspiration (ET), with potential impact on the climate system (including temperatures and precipitation). This feedback is frequently overlooked, although it has been demonstrated in both regional and global scale climate models (Maxwell et al., 2007; Lo & Famiglietti, 2011; Campoy et al., 2013; Wang et al., 2018; Ducharne et al., submitted). The large residence time of GW may also increase the Earth system’s memory, with consequences on the persistence of extreme events, hydro-climatic predictability, and anthropogenic climate change, particularly the magnitude of regional warming.

Here, our main goal is to explore the impacts of GW-SM interactions on historical and future climate, by comparing integrations from three different climate models used in CMIP6 (Coupled Model Intercomparison Project Phase 6, Eyring et al., 2016). Their land surface component explicitly describe the spatio-temporal dynamics of GW with GW-SM interactions, but these processes are based on different physical assumptions representative of the state of the art (e.g. scale of GW flow, active depth, input parameters, see a full review in Gleeson et al., 2019). For each climate model, we compare two transient land-atmosphere simulations, one with GW-SM interaction, and a reference simulation, where the related processes are deactivated. Each transient simulation covers 1980-2100, using the SSP5-8.5 radiative forcing after 2015 (O’Neill et al., 2016). The required sea forcing, identical for each transient simulation, comes from observations for 1979-2014, and is deduced from an SSP5-8.5 fully coupled (land-ocean-atmosphere) CNRM-CM simulation.

Within this framework, we want to assess the sensitivity of the simulated climate to GW-SM interaction in a systematic way, by trying to identify robust features among the three models. Our main objectives are twofold: (1) Compare GW-SM and REF simulations to observations to assess if accounting for GW related processes improves some simulated land or climate parameters; (2) Compare future and historical periods to assess if the GW-SM interaction is able to alter the manifestations of climate change. For instance, can we get weaker regional warming in areas with significant GW-SM interactions? The projected simulations have been performed (deliverable D3.1), but their analysis is still preliminary, and has mostly focus on the IPSL simulations, with complementary offline simulations, i.e. driven by a prescribed meteorological forcing.

2. Numerical design

2.1 Models

The three IGEM climate models used in this work are restricted to their land surface and atmosphere components. They correspond to the same models as used in Ducharne et al. (submitted) with prescribed water table depths (WTDs), except for the evolutions developed between CMIP5 and CMIP6.

2.1.3 IPSL-CM6

The land-atmosphere model used here is a subset of the IPSL-CM6 model (Boucher et al., 2020), restricted to the land-surface and atmospheric components, as evaluated under the CMIP6 configuration by Cheruy et al. (2020). This model is run at the 144x142 horizontal resolution (2.5°x1.3°), with 79 vertical levels.

In the standard version of ORCHIDEE, the land surface component of the IPSL climate model, the sole effect of GW is on river discharge (Krinner et al., 2005, Ducharne et al., in prep). This effect is brought by the routing scheme, which define one linear reservoir in each grid-cell to represent GW storage and base flow, with no GW flow between grid-cells, and no feedback on local soil moisture (SM). To describe this feedback, we introduced a new subgrid fraction, corresponding to the lowland parts of the grid-cell, and acting as a buffer between the upland areas, supplying most GW recharge, and the river system eventually draining GW flow. For simplicity, this fraction is constant over time in each grid-cell, and prescribed from a global-scale wetland map recently designed for this purpose at the 500-m resolution (Tootchi et al., 2019). This map (Figure 1) overlaps two classes of wetlands, viz. regularly flooded wetlands (RFWs) from open-water and inundation datasets, and groundwater-driven wetlands (GDWs) derived from high-resolution GW modeling (Fan et al., 2013), and the resulting total wetland extent is 22 % of the global land area (excluding Antarctica and Greenland). This value is among the highest ones in the literature, along with recent estimates also recognizing the contribution of GDWs. The lowland fraction of each grid cell is described as a separate hydrological element, with physically-based water flow relying on a fine vertical discretization (22 soil layers). It is effectively wet when/where GW flow is sufficient, in which case a water table can build up, and feed base flow to the river, as well as enhanced evapotranspiration compared to the upland fraction, where the 2-m soil is disconnected from the (deep) water table. For the time being, the land cover is assumed to be the same in the upland and lowland fraction, by lack of clear guiding rules to do otherwise (Fan et al., 2019).

This new version is called ORCHIDEE-GWF (GW-fed Fraction), it was detailed and evaluated in the Seine river basin by Tootchi (2019), and we analyze here its impact on the climate simulated by the IPSL-CM6 climate model, by comparison with a reference simulation REF using the standard version of ORCHIDEE (effect of GW on river discharge, but no effect on SM and ET). It must also be underlined that, for the sake of simplicity, several options have been turned off in both versions ORCHIDEE, since they may have interacted with the studied GW-SM interactions. In particular, the simulations do not account for river flooding nor soil freezing in permafrost areas. Plant phenology, however, is prognostic, so the LAI evolves as result of photosynthesis, itself coupled to transpiration.

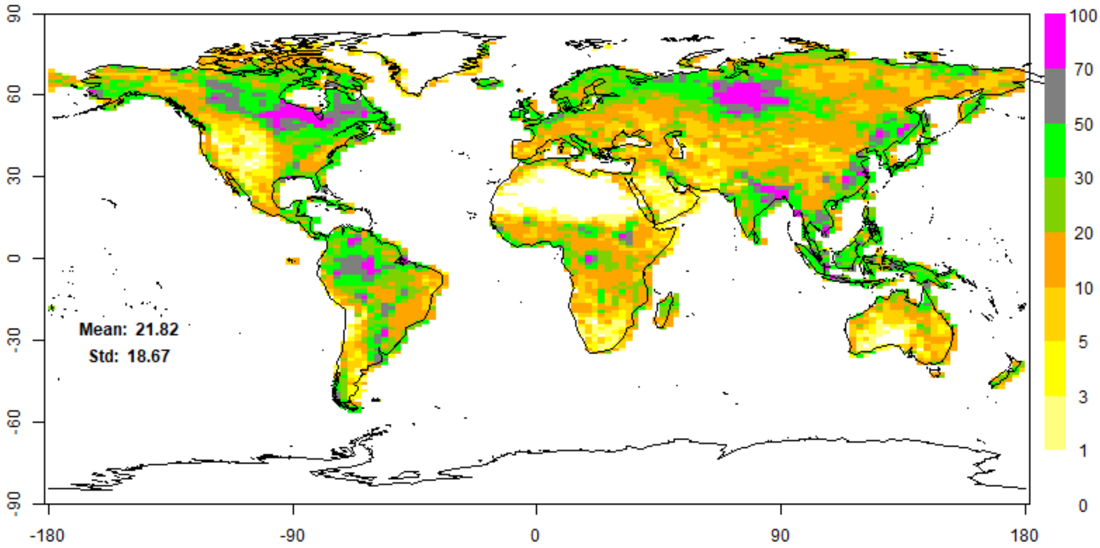

Figure 1. Map of the lowland fraction (in % of land area in each grid cell) used in the IPSL-CM6 simulation with ORCHIDEE-GWF. Upscaled from Tootchi et al (2019) to the 2.5° x 1.3° resolution.

2.1.2 CNRM-CM6

The land-atmosphere model used here is a subset of the CNRM-CM6 model (Voldoire et al., 2019). It is run at a 1.5°x1.5° horizontal resolution (T127 truncation) with 91 vertical levels.

The land surface component is the ISBA-CTRIP model, as recently described and evaluated by Decharme et al. (2019). A mixed form of the Richards equation is used to describe the vertical water-mass transfer within the soil, with 14 layers of increasing thickness down to the 12-m depth. This LSM also includes a 2D diffusive GW scheme, which is used represent horizontal GW flow between grid cells in unconfined aquifers (Vergnes & Decharme, 2012). The latter (Figure 2) are defined based on the global map of the groundwater resources of the world from the Worldwide Hydrogeological Mapping and Assessment Programme (WHYMAP; http://www.whymap.org), and cover 43% of the land surface, excluding Antarctica and Greenland.

The simulated WTD acts as a lower boundary condition for the vertical soil moisture diffusion, a subgrid scale parametrization is implemented owing to the coarse resolution of the grid-scale: it is assumed that upward capillary fluxes from the aquifer can only take place in lowlands of the grid-cells (flat valleys and alluvial plains), where the WTD is shallow enough (Vergnes et al., 2014). The fraction over which capillary rise effectively occurs (f_{wtd}) is derived over time in each grid-cell including an aquifer, by comparing the mean WTD to the accumulated normalized distribution of high-resolution elevation inside the grid-cell, based on a 7.5-arc-second (~250 m) DEM (GMTED2010; Danielson & Gesch, 2011). The water table, in the simulated aquifers, is drained by the rivers and contributes baseflow to the routing scheme. This GW scheme is turned off in the reference simulation to assess the effect of GW-SM on the simulated climate, so this reference simulation includes does not include any GW process (no capillary rise to the soil, no baseflow contribution to the river discharge). River-floodplain interaction, however, is activated in both versions.

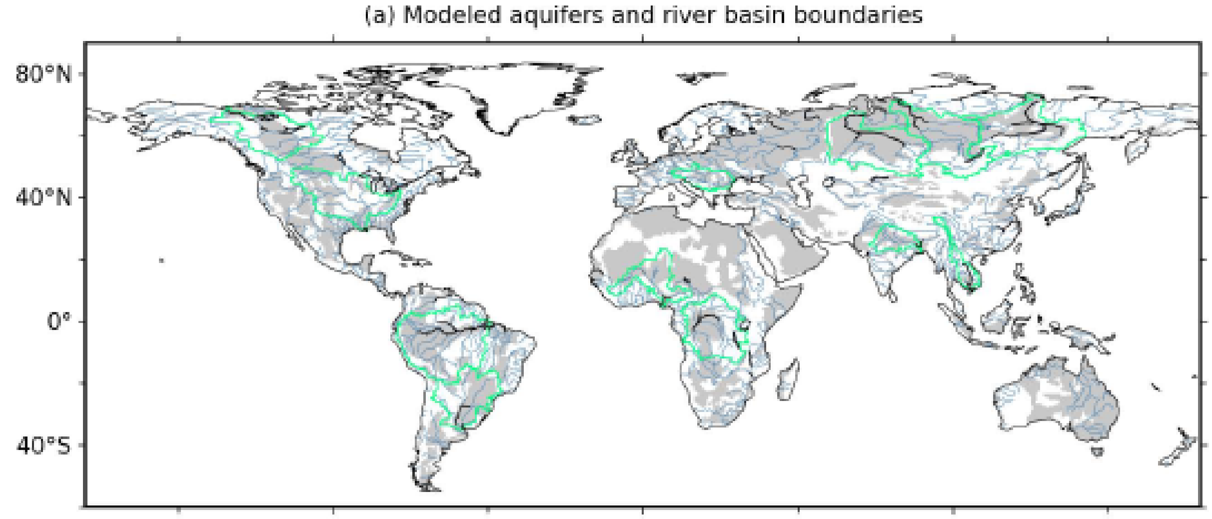

Figure 2. Modeled aquifers (in grey) and river basin boundaries (in green) in the CNRM-CM6 model. From Vergnes & Decharme (2012).

2.1.1 CESM2

The land-atmosphere model used here is a subset of the CESM2 climate model (Danabasoglu et al. 2019). It is run at a 1.9°x2.5° horizontal resolution with 30 vertical layers.

The land surface component is the Community Land Model version 5 (CLM5, Lawrence et al., 2019), but for the sake of comparison with the simulations performed for the Task 1 of the IGEM project (Ducharne et al., submitted), and the ones analyzed in the first ever assessment of GW on the simulated precipitation (Lo & Famiglietti, 2011), the new GW scheme of Swenson and Lawrence (2015) used in CLM5 has been replaced by the GW scheme of Niu et al. (2007), used in CLM versions 2 to 4. This GW scheme defines a conceptual aquifer layer below the 3.8-m soil column, where vertical water flow is classically calculated based on Richards equation, discretized into 10 soil layers. The conceptual aquifer is considered as one layer with a specific yield Sy = 0.2, and an exponentially decaying hydraulic conductivity.

The WTD evolves at each time step as a result of recharge from the soil (which can be negative if the upward capillary flux from the water table is larger than the downward drainage from the unsaturated soil), and baseflow from the saturated layer(s), which contributes to the simulated river discharge. If the water table position is below the 3.8-m soil, capillary rise is deduced from the hydraulic head gradient between the soil bottom and the water table. This GW is purely 1D vertical, with no GW flow between grid-cells, and no subgrid scale variability of capillary rise, which occurs over the full land fraction of each grid-cells. The reference simulation to assess the effect of GW-SM on the simulated climate has no conceptual aquifer layer, so the boundary condition at the bottom of the 3.8-m soil is gravitational drainage (no capillary flux).

2.2 Land-atmosphere simulations over 1979-2100

To reduce the sources of differences between climate models, we focus on land-atmosphere simulations, all performed under the protocol of the Atmospheric Model Intercomparison Project (AMIP), with prescribed interannually-varying forcing boundary conditions from observations (sea surface temperatures - SST, sea ice cover - SIC, greenhouse gases, aerosols, land-use), following Taylor et al. (2012), but updated for the 1979-2014 historical period for CMIP6.

To extend this period over the entire 21st century, we preferred the most severe CMIP6 radiative forcing, namely SSP5-8.5, to get a strong climate change signal at the end of the 21st century. The required SST/SIC forcing datasets have been provided over 2015-2100 by the CNRM (partner P3), and consist of bias-corrected SST and SIC output from a fully coupled (land-ocean-atmosphere) simulation by the CNRM-CM6 climate model, performed for ScenarioMIP (O'Neill et al., 2016) under historical then SSP5-8.5 radiative forcing. To prevent from inhomogeneities in climate variability between the historical and future periods (respectively constrained by observed SST in AMIP, and modeled bias-corrected SST under SSP5-8.5), the future simulations were preceded by historical simulations forced with an equivalent SST/SIC forcing, i.e. modelled by the fully coupled CNRM-CM6 climate model under observed historical radiative forcing, then bias-corrected with the same method as used to prepare the future SST/SIC forcing.

Eventually, we performed three pairs of transient simulations with each land-atmosphere (LA) model involved in the IGEM project, each pair comprising a simulation with GW-SM interactions, and a reference one, REF, where the related processes are deactivated:
1) AMIP simulations, over 1979-2014, well suited for validation since the inter-annual climate variability is well constrained by the observed SST forcing;
2) LA-Historical simulations, over 1979-2014, which only differ from the AMIP simulations by their modelled bias-corrected SST/SIC forcing;
3) LA-Future simulations over 2015-2100, directly pursuing the LA-Historical simulations, and forced by radiative forcing from SSP5-8.5, and by corresponding modeled bias-corrected SST/SIC.

The spin-up (to initialize the AMIP and LA-Historical simulations in 1979) was let to each groups' expertise.

It must be noted that, contrarily to the classical AMIP protocol, we kept a constant land-cover in all land-atmosphere simulations throughout the entire period (1979-2100) so the climate change signal is simple, and the possible attenuation of warming by GW does not involve feedbacks via land-cover change. Each land cover map is representative of the early 21st century conditions, from the datasets used for CMIP6 by each model. Each model used its standard soil texture map, and the corresponding soil hydraulic parameters.

2.3 Complementary off-line simulations with ORCHIDEE

A pair of REF and GW-SM simulations was also performed in off-line mode over 1979-2010 (32 years, after a 20-yr warm up) with the ORCHIDEE LSM, as a complement to the ISPL-CM6 land-atmosphere simulations. The two off-line simulations were forced with the same soil and land cover maps as the land-atmosphere ones. The meteorological forcing is the one used for the IGEM T1 simulations (Ducharne et al., submitted), based on the 1°x1° and 3-hourly dataset developed by the Princeton University [*Sheffield et al.*, 2006], by downscaling and bias-correcting the National Center of Environmental Prediction National Center for Atmospheric Research (NCEP-NCAR) reanalysis. The 3-hourly precipitation from *Sheffield et al.* [2006] is further hybridized to match the monthly means from the Global Precipitation Climatology Center (GPCC) Full Data Product V6 [*Schneider et al.*, 2011, 2014].

3. Results

3.1 Off-line evaluation of the ORCHIDEE-GWF version

3.1.1 Sensitivity to GW-SM interactions

Figure 3a shows the simulated WTD in the lowland fractions, with white values if there is no WTD along the entire simulation, thus in very arid areas (Sahara). As expected, the WTD is very shallow (blue) in wet climates, much deeper (yellowish) in arid zones. In semi-arid climates, deep WTDs are often found in places with very large lowland fractions (see Figure 1), for instance in the Sahelian band (inner Niger delta, around lake Chad, and in the Sudd Swamp), or in the Ob basin, because the relative contribution from the upland is smaller than in the surrounding places with smaller lowland fraction, thus too small to induce a shallow water table. Since these areas are notorious wetlands, it may be postulated that they are sustained by large scale water flows, and that 2D water redistribution, owing to river flooding and/or 2D GW flow, may be lacking in the simulation.

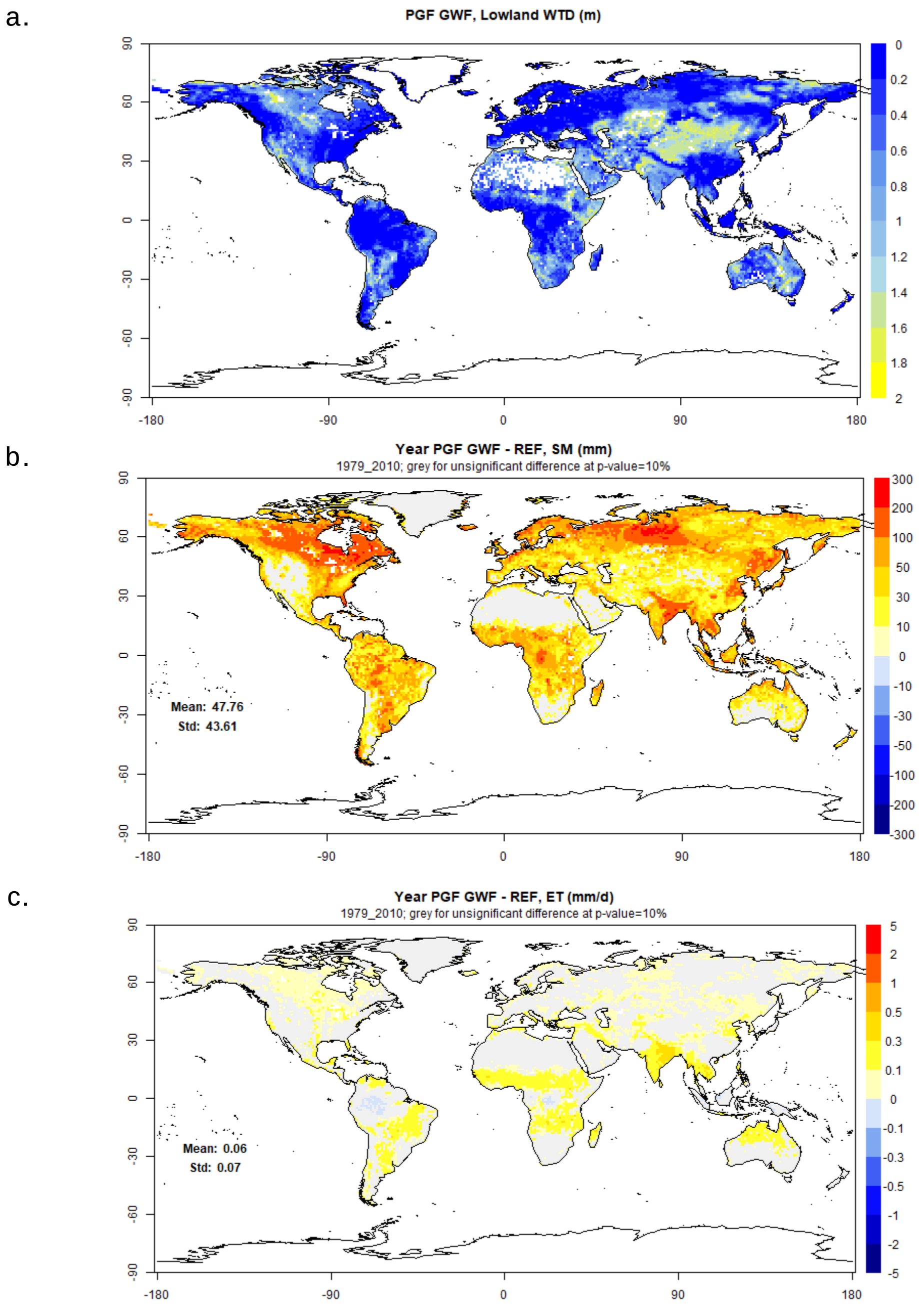

Figure 3. Multi-annual mean differences between the GW-SM and REF simulations with the ORCHIDEE LSM (off-line simulations). Grey shows areas with unsignificant mean changes based on a Student test, with a p-value < 10%.

These scaling problems vanish when looking at grid-cell mean SM, which is everywhere increased by GW flow convergence from upland to lowland (Figure 3b), particularly where the lowland fraction is high (boreal, coastal, and tropical humid areas), with an average of +11% over land. As a result, ET also increases with ORCHIDEE-GWF (+5% on average over land), mostly in transition zones (Figure 3c), where ET is both water limited and not energy limited. In contrast, several areas with a large SM increase with ORCHIDEE-GWF do not show significant ET increases: the boreal areas since water is not limiting in these energy limited areas, and reversely, tropical humid areas, like the Amazon and Congo river basins, or the maritime continent, where ET is not water limited despite the high net radiation. ET is even found to decrease in these areas, which is probably related to the dynamic LAI in this model, via the interplay between soil evaporation and transpiration. Both transpiration and soil evaporation increase with SM, but the latter is more effective than the former when SM is high, as it proceeds at potential rate. Therefore, the increase of LAI with SM slows down the increase in ET, because it increases the fraction of the grid-cells contributing to transpiration, and conversely decreases the fraction contributing to soil evaporation.

d.

e.

f.

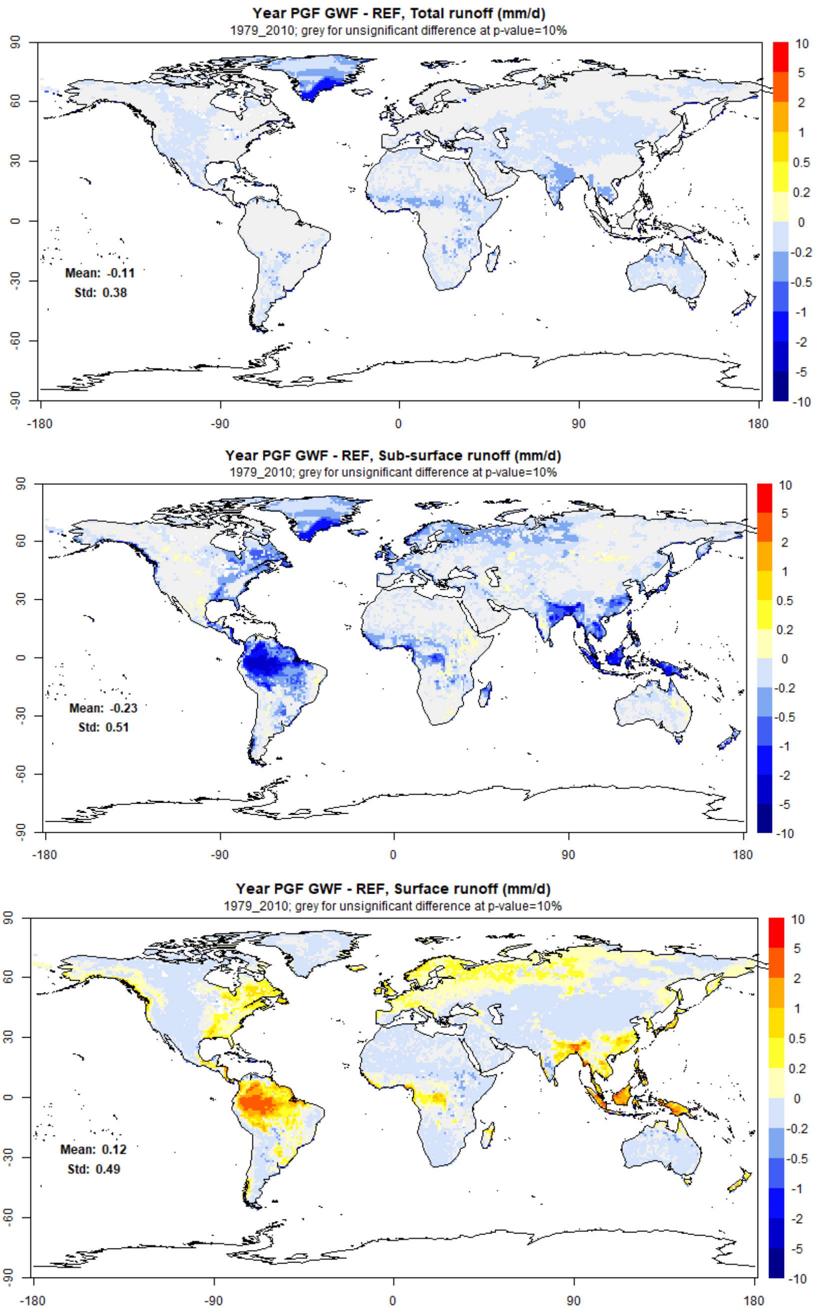

Figure 3 (continued). Multi-annual mean differences between the GW-SM and REF simulations with the ORCHIDEE LSM (off-line simulations). Grey shows areas with unsignificant mean changes based on a Student test, with a p-value < 10%.

Finally, total runoff decreases with ORCHIDEE-GWF (Figure 3d, -11% on average over land), as a direct result of ET decrease in water conservative simulations, both forced by the same precipitation. The rather weak total runoff decrease is the result of much stronger and opposite changes in drainage and surface runoff (respectively -38% and +33% on average over land). Drainage decreases very ubiquitously (Figure 3e), since it is reduced to the baseflow from the lowland water table (the drainage from the lowland fraction becomes a subgrid flux in ORCHIDEE-GWF). Surface runoff shows more contrasted change patterns (Figure 3f), with strong increases where SM increases a lot (humid climates). The SM increase comes from the lowland fraction, which can become very humid, and generate together a water table, and a lot of surface runoff. The decrease of surface runoff in the other land areas has the same explanation as the one of drainage, since the surface runoff produced by the upland fraction is a subgrid flux in ORCHIDEE-GWF, unless it induces surface runoff from the lowland fraction as described above in very humid conditions.

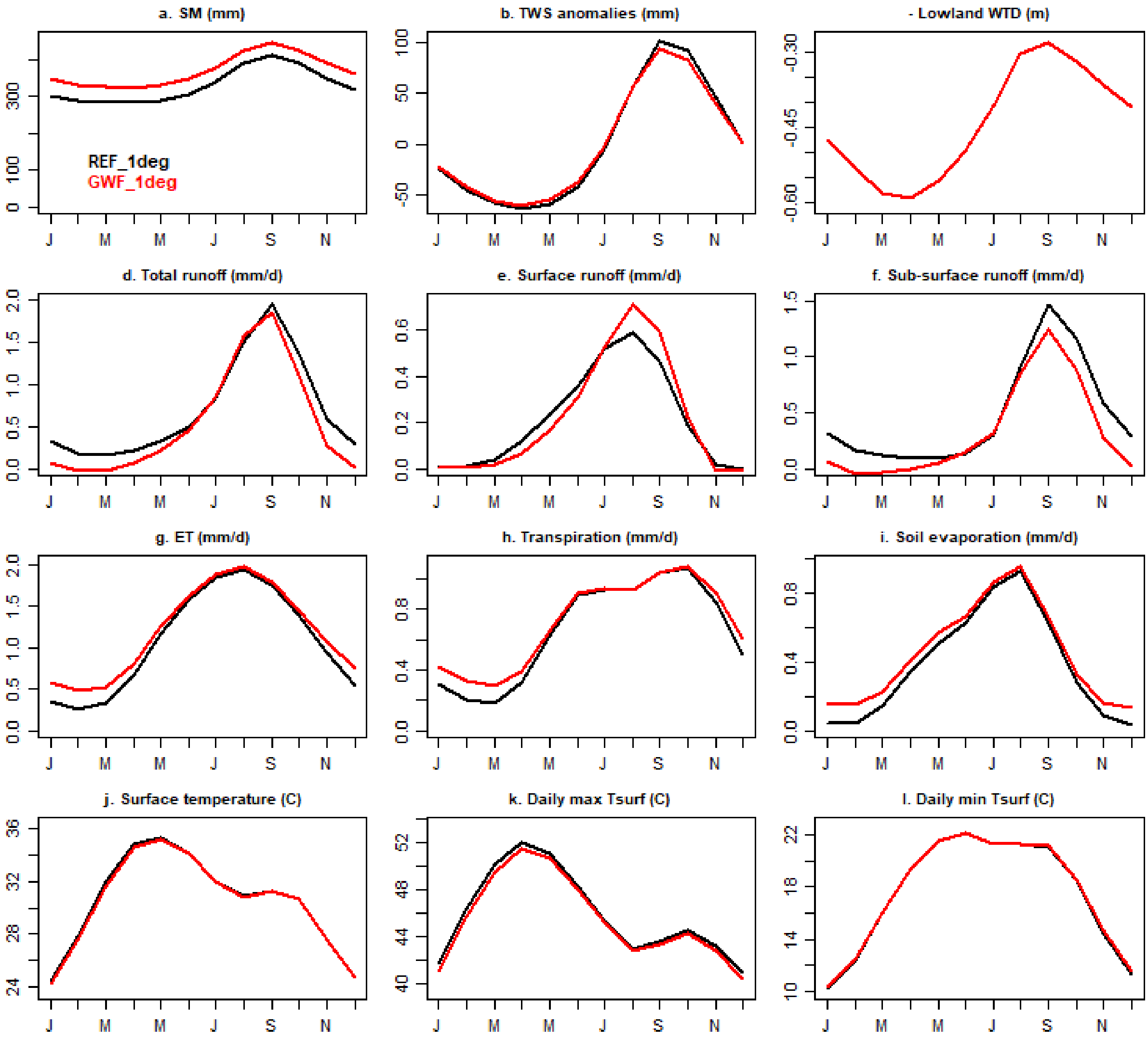

Figure 4. Multi-annual mean seasonal cycles of important land surface variables, on average over the Niger River basin (located in Figure 5a, with an average lowland fraction of 11.8 %). The red and black curves correspond respectively to the GW-SM and REF versions of the ORCHIDEE LSM (off-line simulations over 1979-2010). TWS is the total water storage (given in mm, i.e. kg/m², summing up SM, intercepted water over the canopy, the snow mass, and the water mass in the reservoirs of the routing scheme); this variable is plotted in anomaly with respect to the long-term mean of each simulation.

These hydrological changes also occur seasonally, as illustrated in the Niger river basin (Figure 4), largely overlapping the Sahelian band, where the annual mean changes are amongst the highest over the planet (Figure 3). There the annual mean changes of the main water budget variables between REF and GW-SM are: +11% for SM; +11% for ET; -22% for total runoff, despite a large increase of surface in summer, during the rainy season, from the lowland fraction where the WTD almost reaches the surface (Figure 4c; showing a water table at less than 30 cm from the surface in August and September). We also get a decrease of the surface temperature (Figure 4j, -0.4°C on annual average), with two causes: the increase of ET and related evaporative cooling, but also the one of soil heat capacity with increasing SM. Another noticeable impact is the respective decrease and increase of mean maximum and minimum daily temperature (Figure 4k,l), with an average of -0.85 and +0.5 °C respectively between REF and GW-SM). These variations, which correspond to a decrease of the diurnal amplitude of surface temperature, come from the larger soil heat capacity, soil heat conductivity, and resulting thermal inertia, when the soil is more humid (Aït-Mesbah et al., 2015; Cheruy et al., 2017), as in the lowland fraction.

3.1.2 Evaluation of the simulated river discharge

An important question when developing a new parametrization is to assess if it increases the realism of the model. Following Vergnes & Decharme (2012) for the GW model of the CNRM climate model, we started this work by a comparison to the simulated river discharge (Figure 5).

a

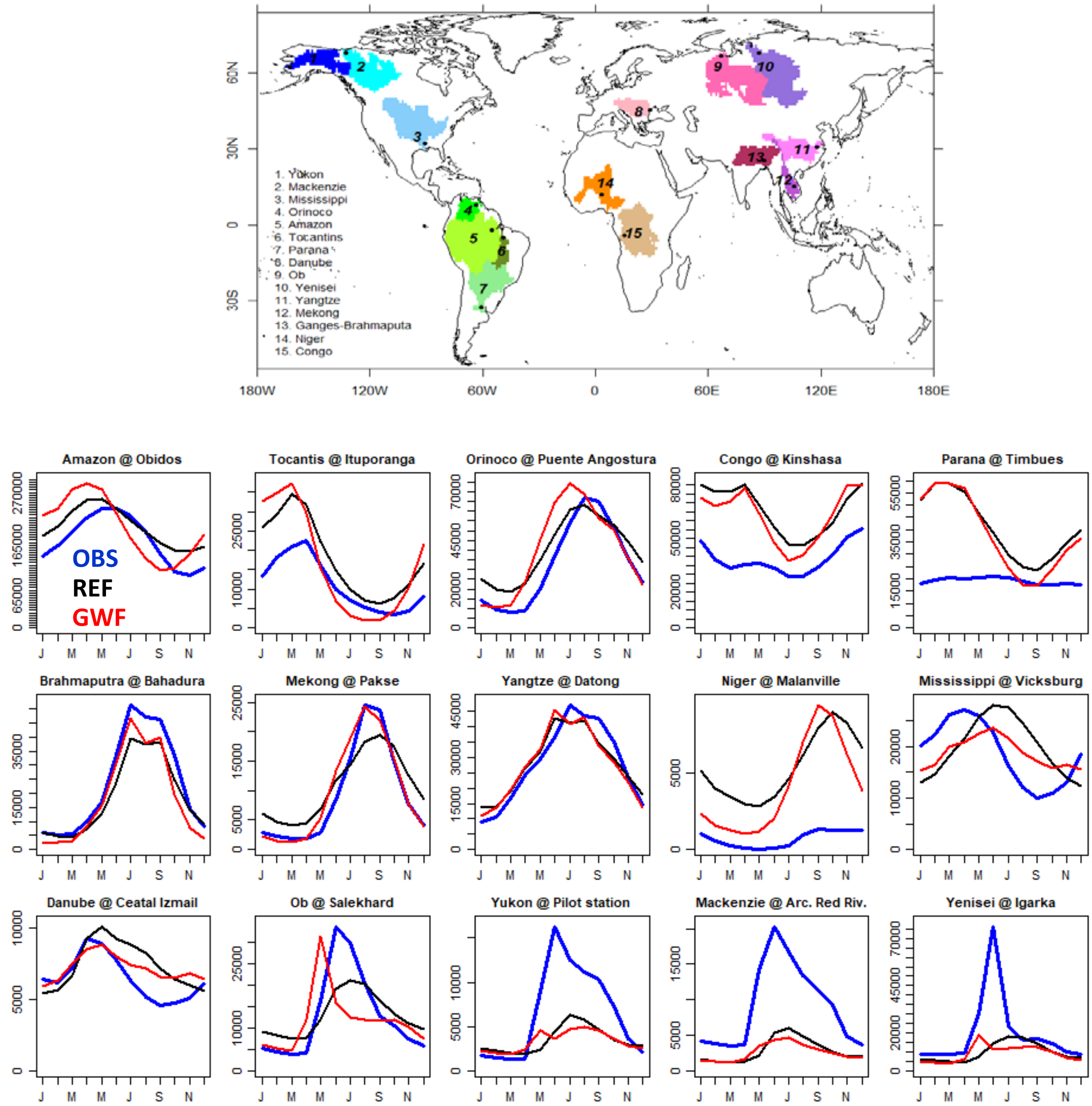

Figure 5. Selected major river basins: a. global map, b. multi-annual mean hydrographs (over 1980-2010) hydrographs, with observations from the Global Runoff data Centre in blue, and offline simulations by the GW-SM and REF versions of the ORCHIDEE LSM in black and red respectively. It must be underlined that the dates with no data in the observed records are censored from the simulated time series, to make the comparison meaningful.

It must be noted, however, that this validation effort still need to be extended to other important land variables, like ET, total water storage anomalies, or surface soil moisture, for which global gridded observation-based products do exist, and also to important atmospheric variables (air temperature, precipitation, radiation), using the land-atmosphere simulations analyzed in section 3.2.

Figure 5 and Table 1 show that the reference ORCHIDEE simulation (in black, with a buffer effect on discharge by the linear GW reservoir of the routing scheme) severely underestimates river discharge of (1) the Niger river, since the inner delta is not accounted, nor the resulting river discharge depletion because of enhanced ET, and (2) the boreal rivers, because the neglect of permafrost favors infiltration and severely reduces runoff. In other river basins, REF compares fairly well with observations, despite significant errors, which may be attributed to several factors: errors in the meteorological forcing, neglect of the significant natural or anthropogenic pressures on river discharge (lakes, dams, and withdrawals), errors in the time constants of the routing scheme, and errors in the simulated water budget.

Looking now at the effect of the GW-SM interaction in the lowland fraction, it is systematically two-fold, with (1) a discharge decrease (because ET increases), (2) advanced peak discharge and low flows, because soil saturation is faster owing to the wet lowlands. Despite exceptions in the Mississippi and Danube, which need further investigation, another significant impact consists of increased seasonal amplitude of river discharge in a majority of basins, likely linked to the second effect, and confirming that accounting for wet areas reduces the effective residence of water in the river basins. This overall effect is also visible in the reduced amplitude of seasonal TWS anomalies in the Niger River basin (Figure 4b), to be confirmed over all land masses, and compared to remote-sensing observation by the GRACE satellite.

Table 1. Performance criteria when comparing the simulated river discharge to the GRDC observations in the selected 15 river basins: relative bias (in %), relative RMSE (in %), relative bias in seasonal amplitude compared to the observation (in %), correlation coefficient between the mean hydrographs (12 mean values for simulation and observation), correlation coefficient between the full time series (excluding the date with no data in the observed record). The evaluated simulations are the same as in Figure 5 (REF and GW-SM versions ORCHIDEE of off-line). The basins are sorted based on their annual mean SM in the river basin in REF (penultimate column), while the last column gives the mean lowland fraction in each basin ($R^2=0.25$ between mean SM and lowland fraction). The green/orange cells indicate basins/criteria for which GW-SM is better/worse than REF.

	RelB%		RelRMSE%		CorClim		CorPluri		RelAmpli%		SM (mm)	Lowland (%)
River@Station	REF	GWF	REF	GWF	REF	GWF	REF	GWF	REF	GWF	REF	
Niger @ Malanville	636,66	471,23	713,06	609,66	0,91	0,76	0,8	0,71	376,99	546,74	329	11,8
Mackenzie @ Arc. Red Riv.	-68,4	-71,19	83,48	87,38	0,88	0,97	0,83	0,87	-70,68	-78,8	414	37,4
Yukon @ Pilot station	-46,87	-49,21	76,47	80,24	0,81	0,83	0,71	0,69	-70,44	-79,41	436	19,8
Mississippi @ Vicksburg	5,06	-0,94	41,06	27,29	0,12	0,52	0,37	0,65	-7,5	-51,94	459	16,2
Yenisei @ Igarka	-49,07	-52,38	98,86	101,02	0,48	0,48	0,45	0,44	-80,24	-78,39	470	22,8
Congo @ Kinshasa	71,21	62,6	75,63	67,58	0,65	0,75	0,54	0,62	30,68	59,76	496	21,0
Ob @ Salekhard	0,7	-8,99	45,23	70,31	0,91	0,46	0,79	0,43	-54,27	-10,51	502	49,2
Brahmaputra @ Bahadura	-20,19	-21,57	28,13	26,49	0,99	0,98	0,95	0,94	-24,89	-4,69	506	42,7
Parana @ Timbues	115,5	101,42	130,78	126,36	0,41	0,39	0,53	0,48	979,17	1175,34	514	27,1
Danube @ Ceatal Izmail	14	10,56	24,97	17,96	0,62	0,8	0,71	0,77	1,14	-38,48	538	15,2
Tocantis @ Ituporanga	63,07	50,6	72,07	91,4	0,97	0,85	0,89	0,78	49,06	86,9	545	29,4
Mekong @ Pakse	16,14	6,1	40,19	20,96	0,95	0,97	0,92	0,95	-32,47	1,64	553	36,6
Yangtze @ Datong	1,1	-0,57	16,2	17,85	0,95	0,92	0,91	0,88	-24,66	-8,89	605	28,5
Amazon @ Obidos	15,36	15,03	18,79	31,97	0,93	0,6	0,9	0,61	-22	31,1	631	37,4
Orinoco @ Puente Angostura	22,78	20,71	30,32	40,43	0,98	0,87	0,96	0,85	-24,39	9,4	666	43,7

In terms of performance, it is not straightforward to assess which version is better, given the often large biases of the reference simulation. This is particularly true in 6 of the 15 selected basins, where the performance changes seem very negligible in front of the errors (Parana, Brahmaputra, Yangtze, and three boreal rivers, namely the Yukon, Mackenzie, and Yenisei). In the remaining nine basins, the GW-SM version tends to improve the simulated volume (cf. bias in Table 1), which is consistent with the improvement of mean simulated ET over land (excluding Greenland and Antarctica): from 1.17 mm/d in REF to 1.23 mm/d in GW-SM, thus closer to state-of-the art observation-based estimates (1.37

mm/d according to GLEAM, Martens et al., 2017; 1.45 mm/d according to Rodell et al., 2015).

a.

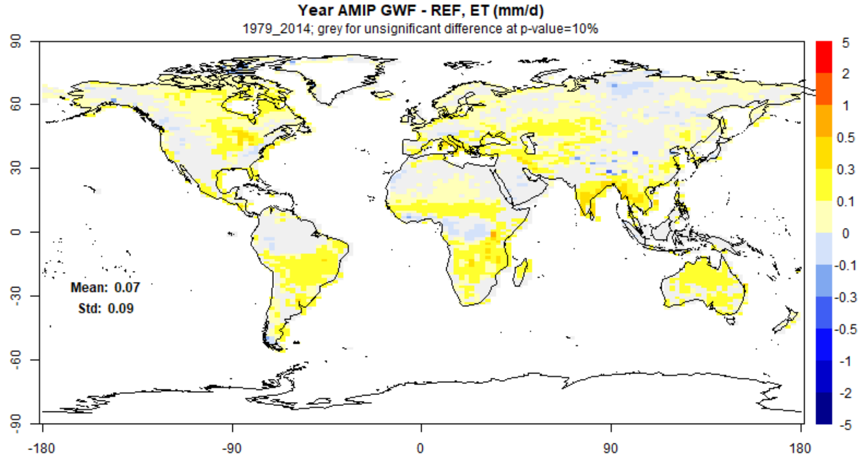

b.

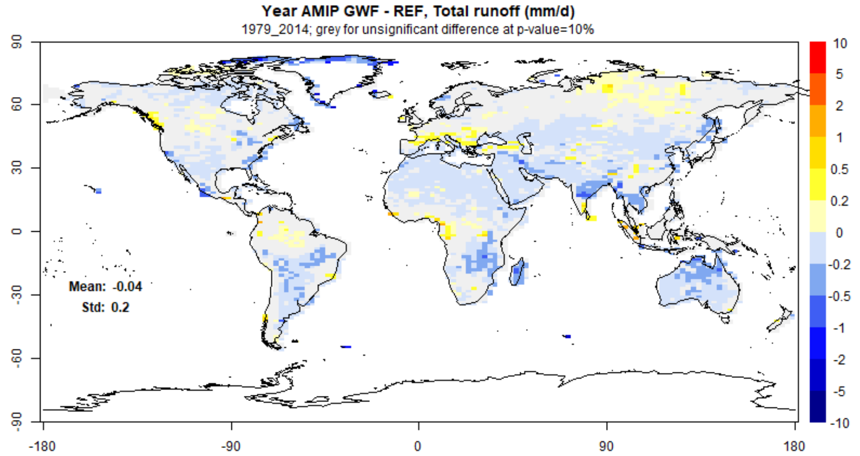

c.

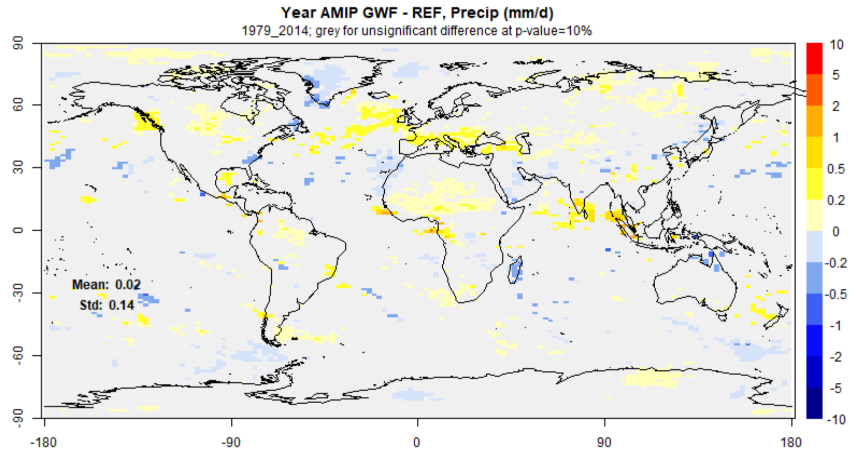

d.

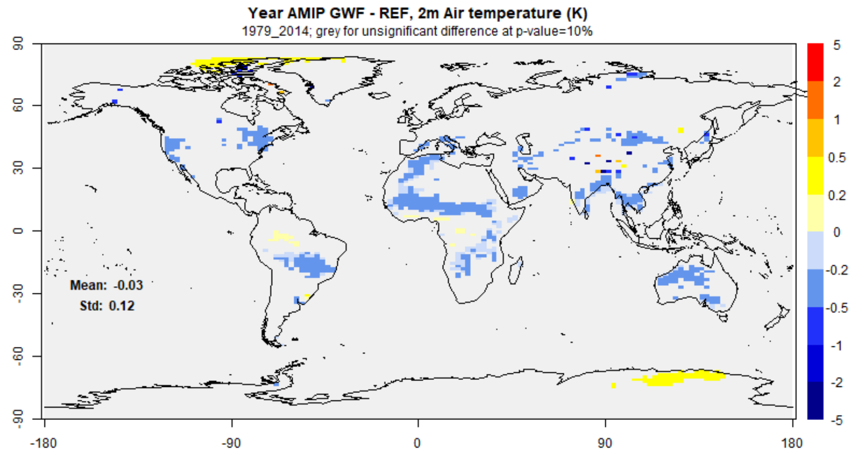

Figure 6. Multi-annual mean differences between the GW-SM and REF simulations with the IPSL-CM6 (land-atmosphere simulations). Grey shows areas with unsignificant mean changes based on a Student test, with a p-value < 10%.

The seasonal amplitude increase with GW-SM interactions represents an improvement in the most humid basins, although the timing of the corresponding hydrographs (cf. correlation coefficients in Table 1) is deteriorated, while the reverse may be speculated in drier basins, where water is limiting, at least seasonally. These associations, although sensible from a physical point of view, need to be verified across a larger sample of river basins.

3.2 Impact of GW-SM interaction on the simulated climate

3.2.1 Historical climate (AMIP simulations)

Over the historical period, the impact of GW-SM interactions on the simulated ET by the ORCHIDEE LSM is very similar in forced and coupled (AMIP) modes, although the significant changes seem larger in coupled mode (Figure 6a). In contrast, the total runoff decrease owing to GW-SM interactions (Figure 6b) is much smaller in coupled mode (-2.7% on land average compared to -11% in forced mode), as a result from the feedback of increased ET to precipitation (Figure 6c).

This feedback is mostly positive (thus increasing precipitation, and counteracting the total runoff decrease), but very weak on annual average, although focused significant precipitation increases can be found in some well-known semi-arid/transition zones, like Sahel and the Mediterranean rim. The near surface atmospheric cooling arising from the previously analyzed surface temperature cooling (due to evaporative cooling and increased soil thermal inertia) is also very weak, with multi-annual means of -0.3°C and -0.1°C on average over land and the entire Earth, respectively.

a.

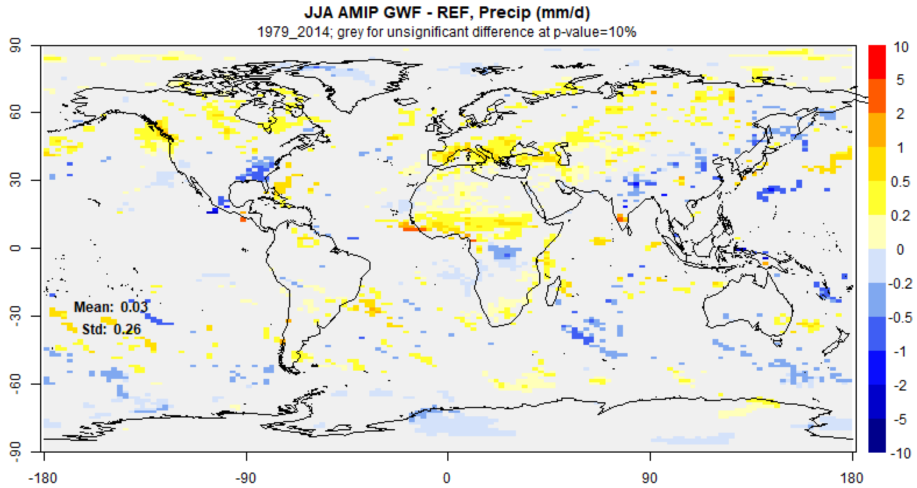

b.

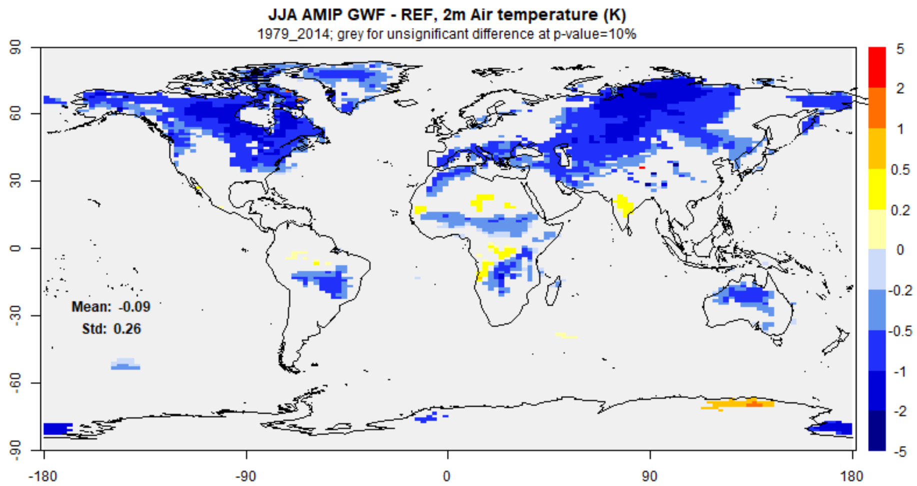

Figure 7. Multi-annual mean differences in boreal summer (June-July-August) between the GW-SM and REF simulations with the IPSL-CM6 (land-atmosphere simulations). Grey shows areas with unsignificant mean changes based on a Student test, with a p-value < 10%.

A stronger impact of GW-SM interactions is found in boreal summer (June-July-August, Figure 7), owing to the larger land masses in the Northern Hemisphere. This leads to a stronger increase of precipitation over the Mediterranean rim and Sahel (Figure 7b) than on a yearly basis. Following the analysis of Wang et al. (2018) with a prescribed 1-m WT, the strong precipitation increase found in JJA over Sahel corresponds to the propagation of the West African monsoon further north into land, due to increased meridional temperature gradient between the equator and higher latitudes, given the much higher and widespread air temperature decrease in the northern middle latitudes (where the cooling can exceed -1°C, especially in areas with high lowland fractions, cf. Figure 1) than around the Equator (Figure 7b).

As shown in Figure 8, this enhancement of the West-African monsoon and the related precipitation corrects a long lasting defect of the IPSL climate model (Cheruy et al., 2020), with a much more realistic GW parametrization (dynamic WTD in selected lowland fractions) than in Wang et al. (2018), in which the WT is uniformly and constantly imposed at 1m from the surface. Besides, the significant cooling found in the boreal areas with GW-SM in JJA is prone to alleviating the warm bias diagnosed in the IPSL-CM6 model by Cheruy et al. (2020) in these areas.

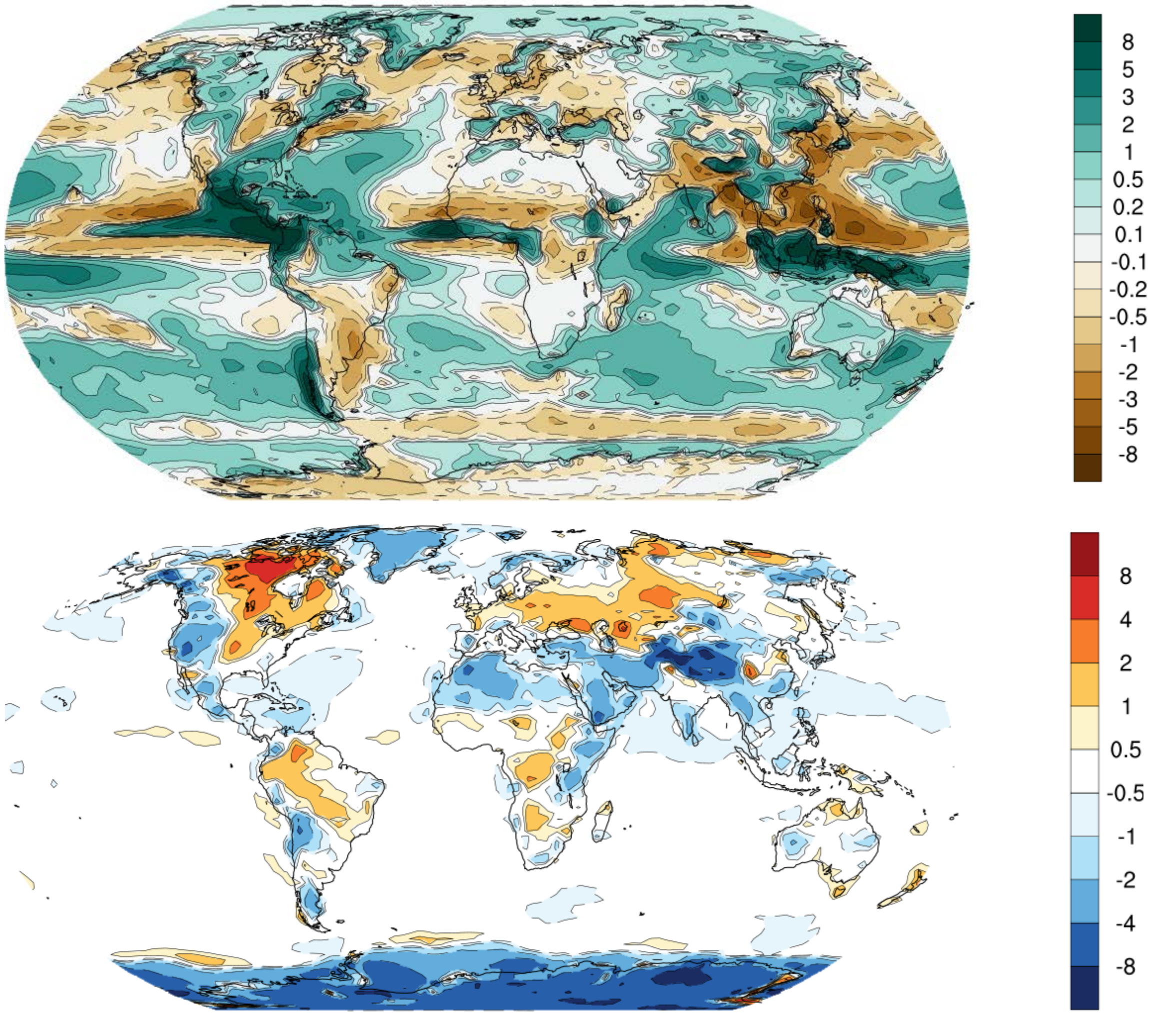

Figure 8. Mean multi-annual bias of the IPSL-CM6 model in JJA: (top) for precipitation, in mm/d, with respect to GPCP observations; (bottom) for 2m-temperature, in °C, with respect to the ERA-I reanalysis. The simulations are performed following the CMIP6 AMIP protocol with a very close version to REF for both ORCHIDEE and the atmospheric model. The biases are calculated over 1979-2014 period. Taken from Cheruy et al. (2020).

The impact of GW-SM interaction, already weak in the IPSL-CM AMIP simulation, is even weaker in the CNRM-CM AMIP simulations, as illustrated for 2-m air temperature in Figure 9, with very tiny spots of significant cooling. The warmer pockets found with GW-SM in arctic areas in DJF are also found in the IPSL-CM simulations (not shown), without any clear explanation for the moment. A thorough comparison of the different model responses is now needed, encompassing the three climate models of the IGEM project, with similar methods, especially for statistical assessment.

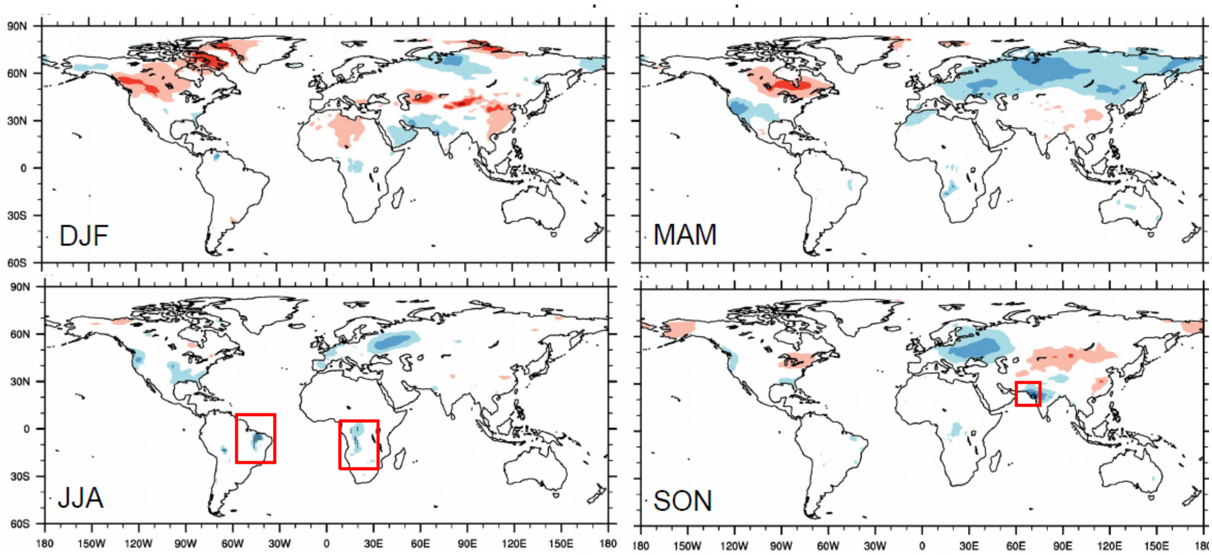

Figure 9. GW impact on mean 2m temperature over the four seasons in the CNRM-CM6 AMIP simulations (multi-annual mean of GW-REF over 1980-2014). Hashed areas correspond to statistically significant differences with a p-value < 5%, using the Wilks (2016) global test, and are highlighted by red boxes.

3.2.2 Future climate

The climate change expected from to the SSP5-8.5 radiative forcing scenario is summarized in Figure 9 for the IPSL-CM simulations, but the large spread of future climate projections must be underlined. For instance, the equilibrium climate sensitivity (ECS, the global surface temperature response to CO_2 doubling) of the CMIP6 climate models ranges from +2°C to almost +6°C, with a multi-model mean ECS around +4.1°C (Zelinka et al., 2020). Based on the same paper, the three fully coupled climate models linked to the IGEM models are in the warmer half, with an ECS of +4.6°C with IPSL-CM6A-LR, +5.2°C with CNRM6-CM6-1, and +5.5°C with CESM2. For the SSP-5.8-5, the spread of global mean increase in 2m air temperature between 1980 and 2100 is approximately between +3.7°C and +7°C (Forster et al., 2020), to be compared with the IPSL-CM6 projection of ca. +6°C (using bias-corrected SST from the CNRM-CM6 model).

Associated to this strong warming, and in line with many other future projections (e.g. IPCC, 2014), the REF simulation performed with IPSL-CM6 shows an increase of precipitation (ca + 8% on average over the entire globe) and an increase in the number of dry days (with precipitation < 1 mm/d) per month (Figure 9). The combination of these two trends is consistent with the intensification of the water cycle, with more precipitation on global average, but concentrated in the wet areas and wet moments, to the detriment of the dry areas and dry moments, as summarized by the "dry gets drier, wet gets wetter" paradigm (e.g. Chou et al., 2013; Greve et al., 2014).

Figure 9 also shows that the impact of GW-SM interaction found over the historical period (section 3.2.1) persists throughout the 21st century: 2-m air temperature remains consistently lower with GW-SM than with REF, and so does the mean of daily maximum temperature (with a larger effect, as previously noted for surface temperature, owing to enhanced thermal inertia); precipitation, in contrast, is higher with GW-SM, logically decreasing the number of dry days. Figure 10 offers a more precise illustration of the effect of the GW-SM interaction on the trend of 2-m air temperature, focused on land masses only (because sea surface temperatures are forced in our simulations). It also compares the response of two models, IPSL-CM6 and CNRM-CM6, which both show a very similar decreasing trend of the temperature difference between GW-SM and REF, meaning that the warming trend along the 21st century is slower in both models when the GW-SM interaction is accounted for.

This mitigation is very weak on average land, since the simulated warming of +6°C over the 21st century is only reduced by 0.1°C over the same period. However, the geographic distribution of the attenuation of anthropogenic warming owing to GW-SM interaction in the IPSl-CM6 climate model (Figure 11) reveals several regions where the projected warming at the end of the 21st century may be significantly reduced, by at least 0.5°C on annual average, like in Western Europe. To summarize, the global mean impact of GW-SM interaction, albeit small on average over land, offers a significant mitigation of climate change in some areas, and the above analysis will shortly be extended to the three climate models, and to a larger number of climate variables, including the number of dry days, and several kinds of extreme event, like heatwaves and droughts (Lorenz et al., 2015; Teuling et al., 2013; Moon et al., 2018; Padron et al., 2020).

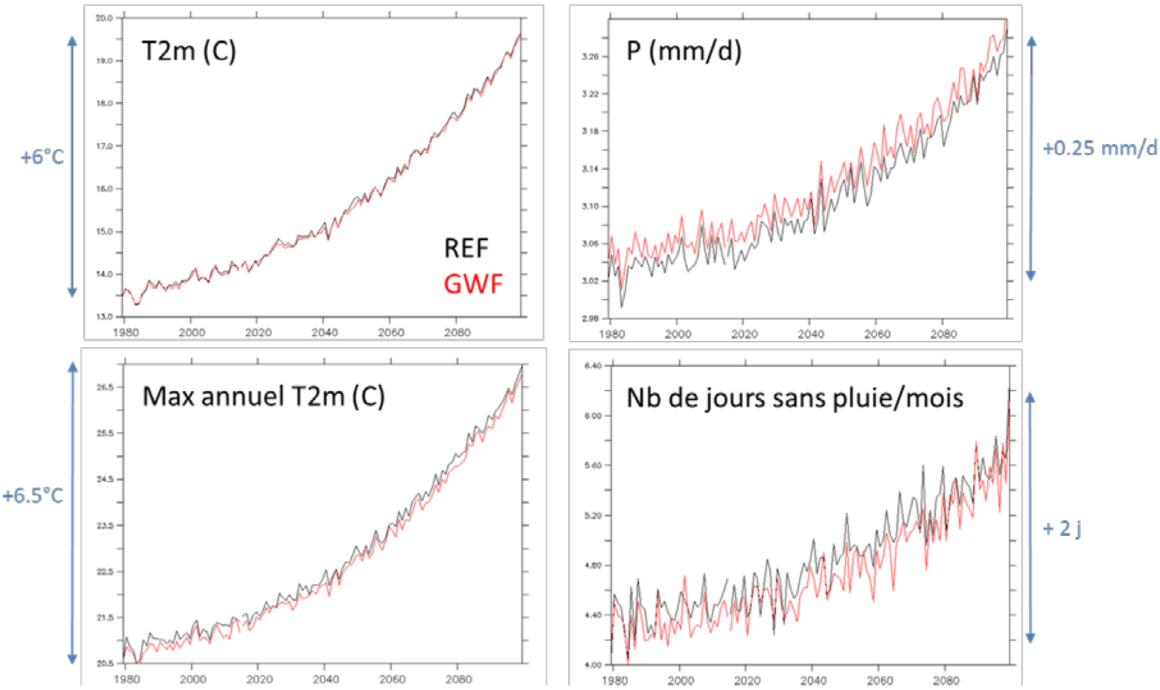

Figure 9. Evolution of yearly means between 1980 and 2100 according to the GW-SM and REF simulations with the IPSL-CM6 LA simulations (global averages).

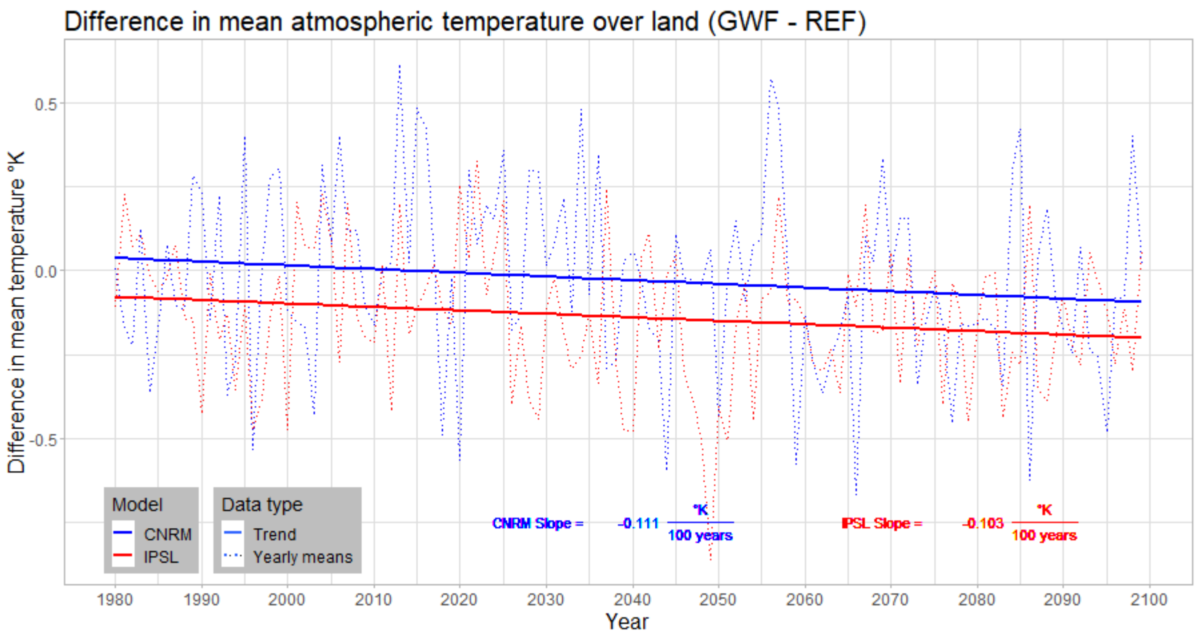

Figure 10. Attenuation of global warming (SSP5-8.5 radiative forcing scenario) on average over land (-0.1°C/100 years) owing to the GW-SM interactions, in simulations with the CNRM-CM6 model (blue) and IPSL-CM6 (red). The trends are extracted based on a linear regression model.

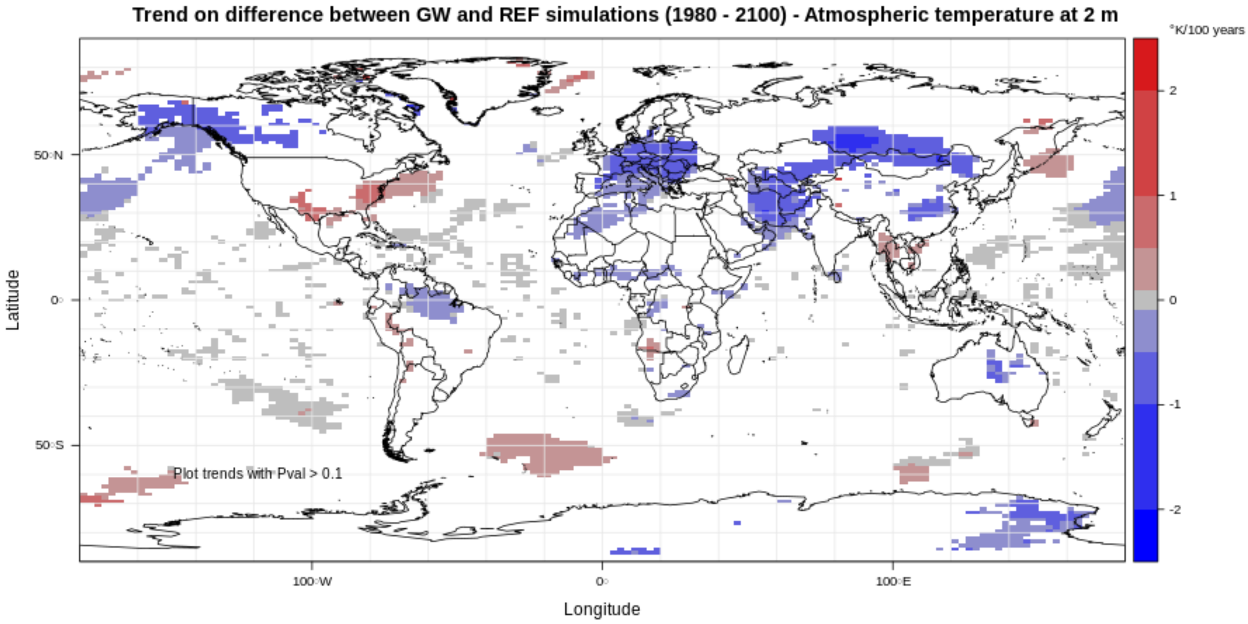

Figure 11. Patterns of global warming attenuation owing to the GW-SM interactions in the IPSL-CM6 simulations (under SSP5-8.5 radiative forcing scenario). This map generalizes to each grid-cell the trend displayed in Figure 10 for the land average of 2-m air temperature difference between GW-SM and REF. Trends (expressed in °C per 100 years) are extracted based on a linear regression model, and the significance is assessed at the 10% level.

4. Conclusions

This report focuses a lot on the IPSL-CM6, for which an original parametrization of GW-SM interactions has been developed during the IGEM project to capture the main effects of hillslope water redistribution in a simple and numerically efficient way. The off-line evaluation of this new model needs to be extended to a wide range of variables, and the results obtained on river discharge (section 3.1.2) call for an improved calibration, for instance by increasing the GW residence time to compensate the earlier peak and low flows, but floodplains and permafrost need to be activated for such a calibration to be meaningful.

At the land surface, the main impacts of GW-SM interaction logically consist of increased SM and ET, and decreased total runoff and surface temperature (direct cooling by ET and larger heat capacity in wet fractions). The subsequent impacts on precipitation and air temperature are weak but significant in some areas, with patterns linked to general circulation, and modulated by lowland fractions and land-atmosphere feedback.

A thorough comparison of the different model responses is now needed, encompassing the three climate models of the IGEM project with similar methods, especially for statistical assessment (e.g. Wilks, 2016). In particular, since the overall sensitivity is weak, a better significance assessment may require ensemble simulations. Important scientific questions will be addressed owing to this multi-model analysis: (i) can we highlight areas where the GW-SM interaction improves the land-surface or atmospheric simulations, although it might be difficult owing to the small sensitivity in front of the large uncertainties of both observations and simulated variables; (ii) do we get weaker regional warming in areas with significant GW-SM interactions? (iii) can this kind of physical mitigation of regional warming be cancelled with increasing land aridity?

Acknowledgements

This work was jointly supported by the Agence Nationale de la Recherche in France (grant ANR-14-CE01-0018-01) and the MoST in Taiwan (grant MOST-104-2923-M-002-002-MY4). The IPSL simulations were performed using the IDRIS computational facilities (Institut du Développement et des Ressources en Informatique Scientifique, CNRS, France).

References

Aït-Mesbah, S., J. L. Dufresne, F. Cheruy, and F. Hourdin (2015), The role of thermal inertia in the representation of mean and diurnal range of surface temperature in semiarid and arid regions, Geophys. Res. Lett., 42, 7572–7580, doi:10.1002/2015GL065553.

Boucher O, Servonnat J, and 76 others (2020). Presentation and evaluation of the IPSL-CM6A-LR climate model. Submitted to JAMES.

Campoy, A., Ducharne, A., Cheruy, F., Hourdin, F., Polcher, J., and Dupont, J.-C. (2013). Response of land surface fluxes and precipitation to different soil bottom hydrological conditions in a general circulation model. *JGR-Atmospheres*, **118**, 10725–10739.

Cheruy, F., Dufresne, J. L., Aït Mesbah, S., Grandpeix, J. Y., & Wang, F. (2017). Role of soil thermal inertia in surface temperature and soil moisture-temperature feedback. Journal of Advances in Modeling Earth Systems, 9, 2906–2919. https://doi.org/10.1002/2017MS001036

Cheruy F, Ducharne A, Hourdin F, Musat I, Vignon E, Gastineau G, Bastrikov V, et 13 others (2020). Improved near surface continental climate in IPSL-CM6 by combined evolutions of atmospheric and land surface physics. Submitted to JAMES.

Cheruy F, Dufresne JL, Hourdin F, Ducharne A (2014). Role of clouds and land-atmosphere coupling in systematic mid-latitude summer warm biases and climate change amplification in CMIP5 simulations, *Geophys. Res. Lett.*, **41**, 6493–6500, doi:10.1002/2014GL061145.

Chou, C., Chiang, J., Lan, C. et al. Increase in the range between wet and dry season precipitation. Nature Geosci 6, 263–267 (2013). https://doi.org/10.1038/ngeo1744

Danabasoglu, G., Lamarque, J.-F., Bacmeister, J., Bailey, D. A., DuVivier, A. K., Edwards, J., et al. (2020). The Community Earth System Model Version 2 (CESM2). *Journal of Advances in Modeling Earth Systems*, 12, e2019MS001916. https://doi.org/10.1029/2019MS001916

Danielson, J.-J., &Gesch, D.-B. (2011). Global multi-resolution terrain elevation data 2010 (GMTED2010). U.S. Geological Survey Open- File Report 2011–1073, 26. Retrieved from https://pubs.usgs.gov/of/2011/1073/pdf/of2011-1073.pdf

Decharme, B., Delire, C., Minvielle, M., Colin, J., Vergnes, J.-P., Alias, A., et al. (2019). Recent changes in the ISBA-CTRIP land surface system for use in the CNRM-CM6 climate model and in global off-line hydrological applications. Journal of Advances in Modeling Earth Systems, 11, 1207– 1252. https://doi.org/10.1029/2018MS001545

Ducharne A, Lo MH, Decharme B, Chien RY, Ghattas J, Colin J, Tyteca S, Cheruy F, Wu WY, Lan CW. Compared sensitivity of land surface fluxes to water table depth in three climate models. Submitted to Journal of Hydrometeorology.

Ducharne, A., Ghattas, J., Maignan, F., Ottlé, C., Vuichard, N., Guimberteau, M., Krinner, G., Polcher, J., Tafasca, S., Bastrikov, V., Cheruy, F., Guénet, B., Mizuochi, H., Peylin, P., Tootchi, A. and Wang, F. Soil water processes in the ORCHIDEE-2.0 land surface msodel: state of the art for CMIP6, in prep pour Geosci. Model Dev.

Eyring, V., Bony, S., Meehl, G. A., Senior, C. A., Stevens, B., Stouffer, R. J., and Taylor, K. E.: Overview of the Coupled Model Intercomparison Project Phase 6 (CMIP6) experimental design and organization, Geosci. Model Dev., 9, 1937–1958, https://doi.org/10.5194/gmd-9-1937-2016, 2016.

Fan, Y., Li, H. & Miguez-Macho, G. Global Patterns of Groundwater Table Depth. *Science* **339**, 940-943, doi:10.1126/science.1229881 (2013).

Fan, Y., Clark, M., Lawrence, D. M., Swenson, S., Band, L. E., Brantley, S. L., et al. (2019). Hillslope hydrology in global change research and Earth system modeling, Water Resources Research, 55, 1737– 1772, https://doi.org/10.1029/2018WR023903

Faroux, S., Kaptué Tchuenté, A. T., Roujean, J.-L., Masson, V., Martin, E., & Le Moigne, P. (2013). ECOCLIMAP-II/Europe: A twofold database of ecosystems and surface parameters at 1 km resolution based on satellite information for use in land surface, meteorological and climate models. Geoscientific Model Development, 6(2), 563–582. https://doi.org/10.5194/gmd-6-563-2013

Forster, P.M., Maycock, A.C., McKenna, C.M. et al (2020). Latest climate models confirm need for urgent mitigation. Nat. Clim. Chang. 10, 7–10, https://doi.org/10.1038/s41558-019-0660-0

Gascoin, Ducharne, Ribstein, Carli, Habets (2009). Adaptation of a catchment-based land surface model to the hydrogeological setting of the Somme River basin (France). *J. Hydrology*, **368**, 105-116.

Greve, P., Orlowsky, B., Mueller, B. et al. (2014). Global assessment of trends in wetting and drying over land. Nature Geosci 7, 716–721. https://doi.org/10.1038/ngeo2247

IPCC (2014). Climate Change 2014: Synthesis Report. Contribution of Working Groups I, II and III to the Fifth Assessment Report of the Intergovernmental Panel on Climate Change [Core Writing Team, R.K. Pachauri and L.A. Meyer (eds.)]. IPCC, Geneva, Switzerland, 151 pp.

Koster, R. D., et al. (2004). Regions of strong coupling between soil moisture and precipitation. *Science, **305**,* 1138-1140.

Krinner, G., N. Viovy, N. de Noblet-Ducoudré, J. Ogée, J. Polcher, P. Friedlingstein, P. Ciais, S. Sitch, and I. C. Prentice (2005). A dynamic global vegetation model for studies of the coupled atmosphere-biosphere system, *Global Biogeochem. Cycles*, **19**, GB1015.

Gleeson T, Wagener T, Cuthbert M, Rahman S, Bierkens MFP, Döll P, Rosolem R, Zipper SC, Bresciani E, Ducharne A, Taylor R, Hill M, Wada Y, Lo MH, Luijendijk E, Maxwell R, Hartmann A, de Graaf I, Oshinlaja N, West C, S. Famiglietti JS, Kollet S, Condon L, Scanlon B, Kim H. Groundwater representation in continental to global hydrologic models (2019). A call for open and holistic evaluation, conceptualization and classification. EarthArXiv.

Lawrence, D. M., et al. (2011). Parameterization improvements and functional and structural advances in Version 4 of the Community Land Model, *Journal of Advances in Modeling Earth Systems*, ***3***(1), M03001.

Lawrence, D. M., Fisher, R. A., Koven, C. D., Oleson, K. W., Swenson, S. C., Bonan, G., et al. (2019). The Community Land Model version 5: Description of new features, benchmarking, and impact of forcing uncertainty. Journal of Advances in Modeling Earth Systems, 11, 4245-4287, https://doi.org/10.1029/2018MS001583

Lo, M.-H., and J. S. Famiglietti (2011). Precipitation response to land subsurface hydrologic processes in atmospheric general circulation model simulations. *J. Geophys. Res. Atmos.,* **116,** D05107.

Martens, B., Miralles, D. G., Lievens, H., Schalie, R. van der, Jeu, R. A. M. de, Fernández-Prieto, D., Beck, H. E., Dorigo, W. A. and Verhoest, N. E. C. (2017). GLEAM v3: satellite-based land evaporation and root-zone soil moisture, Geosci. Model Dev., 10(5), 1903–1925, doi:https://doi.org/10.5194/gmd-10-1903-2017.

Maxwell, R. M., Chow, F. K., Kollet, S. J. (2007). The groundwater–land-surface–atmosphere connection: Soil moisture effects on the atmospheric boundary layer in fully-coupled simulations, Advances in Water Resources, 30, 2447-2466.

Moon, H., Gudmundsson, L., & Seneviratne, S. I. (2018). Drought persistence errors in global climate models. Journal of Geophysical Research: Atmospheres, 123, 3483–3496. https://doi.org/10.1002/2017JD027577

Niu, G. Y., Yang, Z. L., Dickinson, R. E., Gulden, L. E. & Su, H. Development of a simple groundwater model for use in climate models and evaluation with Gravity Recovery and Climate Experiment data. Journal of Geophysical Research: Atmospheres 112 (2007).

O'Neill, B. C., Tebaldi, C., van Vuuren, D. P., Eyring, V., Friedlingstein, P., Hurtt, G., Knutti, R., Kriegler, E., Lamarque, J.-F., Lowe, J., Meehl, G. A., Moss, R., Riahi, K., and Sanderson, B. M.: The Scenario Model Intercomparison Project (ScenarioMIP) for CMIP6, Geosci. Model Dev., 9, 3461-3482, https://doi.org/10.5194/gmd-9-3461-2016, 2016.

Padrón RS, Gudmundsson L, Ducharne A, Lawrence DM, Mao J, Peano D, Krinner G, Kim H, Seneviratne SI (2020). Observed changes in dry season water availability attributed to human-induced climate change. In revision for Nature Geoscience.

Rodell, M., Beaudoing, H. K., L'Ecuyer, T. S., Olson, W. S., Famiglietti, J. S., Houser, P. R., Adler, R., Bosilovich, M. G., Clayson, C. A., Chambers, D., Clark, E., Fetzer, E. J., Gao, X., Gu, G., Hilburn, K., Huffman, G. J., Lettenmaier, D. P., Liu, W. T., Robertson, F. R., Schlosser, C. A., Sheffield, J. and Wood, E. F. (2015). The Observed State of the Water Cycle in the Early Twenty-First Century, J. Clim., 28(21), 8289–8318, doi:10.1175/JCLI-D-14-00555.1.

Seneviratne, Corti, Davin, Hirschi, Jaeger, Lehner, Orlowsky, Teuling (2010). Investigating soil moisture-climate interactions in a changing climate: A review, *Earth-Science Reviews*, **99**, 125-161.

Swenson, S. C., and D. M. Lawrence (2015), A GRACE-based assessment of interannual groundwater dynamics in the Community Land Model, Water Resour. Res., 51, 8817–8833, doi:10.1002/2015WR017582.

Taylor, K.E., R.J. Stouffer, and G.A. Meehl, 2012: An Overview of CMIP5 and the Experiment Design. Bull. Amer. Meteor. Soc., 93, 485–498, doi:10.1175/BAMS-D-11-00094.1

Teuling, A. J., Van Loon, A. F., Seneviratne, S. I., Lehner, I., Aubinet, M., Heinesch, B., Bernhofer, C., Grünwald, T., Prasse, H., and Spank, U. (2013), Evapotranspiration amplifies European summer drought, Geophys. Res. Lett., 40, 2071– 2075, doi:10.1002/grl.50495.

Tootchi, A (2019). Development of a global wetland map and application to describe hillslope hydrology in the ORCHIDEE land surface model, PhD thesis, Sorbonne Université, Paris (PDF).

Tootchi, A., Jost, A., and Ducharne, A. (2019). Multi-source global wetland maps combining surface water imagery and groundwater constraints, *Earth Syst. Sci. Data*, **11**, 189–220, doi:10.5194/essd-11-189-2019, 2019.

Vergnes, J.-P., and B. Decharme (2012), A simple groundwater scheme in the TRIP river routing model: global off-line evaluation against GRACE terrestrial water storage estimates and observed river discharges, Hydrol. Earth Syst. Sci., 16(10), 3889–3908, doi:10.5194/hess-16-3889-2012.

Vergnes, J.-P., B. Decharme, and F. Habets (2014). Introduction of groundwater capillary rises using subgrid spatial variability of topography into the ISBA land surface model, *J. Geophys. Res. Atmos.*, **119**, 11,065–11,086, doi:10.1002/2014JD021573.

Voldoire, A., Saint-Martin, D., Sénési, S., Decharme, B., Alias, A., Chevallier, M., et al. (2019). Evaluation of CMIP6 DECK experiments with CNRM-CM6-1. Journal of Advances in Modeling Earth Systems, 11, 2177– 2213. https://doi.org/10.1029/2019MS001683

Wang, F., Ducharne, A., Cheruy, F., Lo, M.-H., and Grandpeix, J.-L. (2018). Impact of a shallow groundwater table on the global water cycle in the IPSL land-atmosphere coupled model, *Climate Dynamics*, 50, 3505-3522, doi:10.1007/s00382-017-3820-9

Wilks, D.S. (2016). "THE STIPPLING SHOWS STATISTICALLY SIGNIFICANT GRID POINTS" - How Research Results are Routinely Overstated and Overinterpreted, and What to Do about It, BAMS, 97, 2263–2273, https://doi.org/10.1175/BAMS-D-15-00267.1

Zelinka, M. D., Myers, T. A., McCoy, D. T., Po-Chedley, S., Caldwell, P. M., Ceppi, P., et al. (2020). Causes of higher climate sensitivity in CMIP6 models. Geophysical Research Letters, 47, e2019GL085782. https://doi.org/10.1029/2019GL085782